Philosophical Magazine
Publication details, including instructions for authors and subscription information:
http://www.tandfonline.com/loi/tphm20

Dynamic charge-transfer bond-order potential for gallium nitride

Karsten Albe [a] , J. Nord [b] & K. Nordlund [b]

[a] Technische Universität Darmstadt, Institut für Materialwissenschaft, Petersenstr. 23, D-64287 Darmstadt, Germany

[b] Department of Physics, University of Helsinki, P.O. Box 43, FIN-00014, Finland

Version of record first published: 01 Dec 2009.

To cite this article: Karsten Albe , J. Nord & K. Nordlund (2009): Dynamic charge-transfer bond-order potential for gallium nitride, Philosophical Magazine, 89:34-36, 3477-3497

To link to this article: http://dx.doi.org/10.1080/14786430903313708

Philosophical Magazine
Vol. 89, Nos. 34–36, 1–21 December 2009, 3477–3497

Taylor & Francis
Taylor & Francis Group

Dynamic charge-transfer bond-order potential for gallium nitride

Karsten Albe[a]*, J. Nord[b] and K. Nordlund[b]

[a]*Technische Universität Darmstadt, Institut für Materialwissenschaft, Petersenstr. 23, D-64287 Darmstadt, Germany;* [b]*Department of Physics, University of Helsinki, P.O. Box 43, FIN-00014, Finland*

(*Received 31 May 2009; final version received 4 September 2009*)

We present an analytical interatomic potential for gallium nitride which is based on a new environment-dependent dynamic charge-transfer model. The model consists of a short-ranged bond-order potential that accounts for covalent/metallic interactions and an ionic Coulomb potential with effective point charges that are dynamically adjusted. In contrast to established models, these point charges are distance-dependent and vary with the number and type of nearest neighbour atoms. The basic concepts stem from the idea of bond charges. We assume pairwise symmetric charge transfer between atoms of different type forming a bond. Charge contributions of all bonds to an atomic site are weighted and added, yielding the effective charge per atom. Mulliken charges, as obtained from density-functional theory calculations within the local-density approximation, are used for adjusting the parameters and functional form of the potential. The short-range contributions are chosen as angular-dependent many-body bond-order potentials, which can be understood as an extension of a Finnis–Sinclair type potential.

Keywords: computer simulation; ionic compounds; interatomic potential; molecular dynamics

1. Introduction

Analytical interatomic potentials are widely used for atomic-scale simulations that involve large systems and long time-scales and therefore cannot be treated by computationally more demanding quantum mechanical methods. For metals, alloys, and semi-conductors, a number of cluster potentials and environment-dependent cluster functionals, such as various bond-order, (modified) embedded-atom or Finnis–Sinclair type potentials, have been developed and successfully applied over the last decades [1]. On the other hand, ionic solids are usually described by potential models based on the assumption of fully ionic models with ionic polarisabilities [2,3] and constant effective charges. In case of semi-ionic systems, these potentials are usually complemented by pair or many-body potentials that account for the short-range chemical interaction.

Many physical processes in chemistry, biology and materials systems, however, involve charge-transfer processes that depend on the local atomic environments.

*Corresponding author. Email: albe@mm.tu-darmstadt.de

ISSN 1478–6435 print/ISSN 1478–6443 online

DOI: 10.1080/14786430903313708
http://www.informaworld.com

If fixed charges are used in simulations, they reflect average or mean field charge values of a particular phase, but cannot respond to variations of the electrostatic fields which arise from atomic movements, phase transitions, variations of oxidation states, chemical reactions, kinetically induced disorder, irradiation effects, etc. Moreover, fixed charge models do not assure charge neutrality, if the composition of the simulated ensemble varies. This can also lead to misinterpretations of the lattice energies, since fully separated atoms stay ionised. Thus, refined concepts are needed for understanding and modelling charge redistribution. In the past, the charge equilibration formalism (QEq), based on the concepts of electronegativity equalisation, self-Coulomb repulsion and Coulomb interaction [4–9], has been the key ingredient of most variable-charge models.

A successful implementation of a charge-dependent energy model for alumina was presented by Streitz and Mintmire [10–12] and also parametrised for titania [13] by combining the QEq method with an embedded-atom potential. Recently, an improved version of this scheme was presented by Zhou et al. [14] which allows us to describe metal oxides consisting of more than one metal element. A variant of the QEq method is also used in the ReaxFF approach, where a core charge with fixed positive amplitude is centred on an atom, and a valence charge described as a Gaussian with negative amplitude is allowed to move off the nuclear centre [15,16]. However, Thomas et al. pointed out that in QEq models complemented by short-range Morse potentials, shielding effects lead to significantly weaker electrostatic contributions than fixed charge models [17,18]. Since the choice of the short-range terms determines directly the transferability of such potentials, recent attempts have been made to combine the QEq methods with established many-body potentials. Yasuka [19] proposed an empirical approach that combines the Si-Tersoff potential with effective charges as determined from the QEq method and was later adopted for various ionic compounds [20,21]. An extension of the second-moment tight binding approximation (SMTB+QEq) to partly ionic systems has recently been presented for the case of TiO_2 and ZrO_2 [22] based on the alternating lattice model [23].

A general feature of potentials using the QEq model is that they are computationally demanding in molecular dynamics simulations, since the charges are calculated from an energy minimisation algorithm at every time step. Although effective charges can change as an atom moves, they do not affect the calculation of forces and stresses. This is a very useful feature if the potential model is implemented within a MD code. However, atoms will remain ionic even at separations where they are supposed to return to a neutral state and, as recently pointed out by Zhou and Doty [24], total energy is not conserved in MD-simulations, since the energy minimisation is done without a self-consistent adjustment of the interatomic forces. This can be avoided if alternative functional forms are used that explicitly account for the distance dependence of charge transfer. A phenomenological approach was presented by Alavi et al. [25] for modelling silica. They calculated the effective charges of the Coulomb potential as a linear sum of nearest neighbour contributions using smooth step-functions, and added an empirical pair potential to account for repulsion and covalent interaction. In a similar spirit, Jiang and Brown [26] constructed a potential for the same system, but included three-body terms taken from the silicon potential of Stillinger and Weber [27]. Another analytic charge-transfer scheme was recently proposed by Muralidharan et al., where

the effective charges were also taken as arguments for an embedding function of EAM type [28].

In the past, we have shown that bond-order potentials of the Tersoff–Brenner type are sufficiently flexible to not only describe covalent materials, like Si and C [29], and compound semi-conductors, like GaAs and GaN [30,31], but also fcc [32] and bcc metals [33,34]. This is because they are, in principle, an angular-dependent variant of the second-moment tight binding approximation [32,35] and can therefore be understood as an extension of a Finnis–Sinclair type potential [36].

In this paper, we introduce a dynamic charge-transfer model and corresponding bond-order potential ('DCT-BOP') that represents an alternative implementation of the valence bond method, but rests on an analytical functional form by combining a short-ranged bond-order potential with an electrostatic term. The distance and coordination dependence of the effective charges is based on the Mulliken analysis. The model is derived for GaN but might be transferable to oxide systems, too.

2. Potential model

The purpose of this work is to derive a potential model that can be applied to mixed covalent(or metallic)-ionic materials, covering the essential features of interatomic interactions. To begin with, we write the total cohesive energy of the compound material as

$$E = E_{\text{bonded}} + E_{\text{es}}, \tag{1}$$

where E_{es} accounts for the electrostatic contribution to the total energy, while E_{bonded} describes the repulsive and the chemical interaction energies due to metallic or covalent bonds.

2.1. *Bonded interaction*

Chemical and repulsive interactions are described by a well established bond-order formalism that has been applied to a number of different compound systems [29,32,37] before and is only briefly sketched here. The non-electrostatic contributions are written as a sum over individual bond energies of an ensemble of atoms located on position $\boldsymbol{r}_i$,

$$E_{\text{bonded}} = \sum_{i>j} f_C(r_{ij})\left[V_R(r_{ij}) - \underbrace{\frac{b_{ij}+b_{ji}}{2}}_{\overline{b_{ij}}} V_A(r_{ij})\right], \tag{2}$$

with $r_{ij} = |\boldsymbol{r}_i - \boldsymbol{r}_j|$ and the pairwise attractive and repulsive contributions given by

$$V_R(r) = \frac{D_0}{S-1}\exp\left(-\beta\sqrt{2S}(r-r_0)\right) \tag{3}$$

and

$$V_A(r) = \frac{SD_0}{S-1}\exp\left(-\beta\sqrt{2/S}(r-r_0)\right). \tag{4}$$

Here, D_0, S, β and r_0 are adjustable parameters. The cutoff function

$$f_C(r) = \begin{cases} 1 & r < R - D \\ \frac{1}{2} - \frac{1}{2}\sin\left(\frac{\pi}{2}\frac{r-R}{D}\right) & |R - r| \le D \\ 0 & R + D < r \end{cases} \tag{5}$$

restricts the interactions to the first neighbour shell. The parameters R and D specify the position and the width of the cutoff region. The bond-order is given by

$$b_{ij} = \left(1 + \chi_{ij}\right)^{-1/2} \tag{6}$$

with

$$\chi_{ij} = \sum_{k(\neq i,j)} f_C(r_{ik}) \exp\left[2\mu(r_{ij} - r_{ik})\right] g(\theta_{ijk}) \tag{7}$$

and the angular function

$$g(\theta) = \gamma\left(1 + \frac{c^2}{d^2} - \frac{c^2}{d^2 + [h + \cos\theta]^2}\right). \tag{8}$$

The three-body interactions are determined by the parameters 2μ, γ, c, d and h, which leads in total to up to nine adjustable parameters all of them depending on the type of atoms i and j.

2.2. *Electrostatic interaction*

The electrostatic energy of N interacting ions located at different positions $\boldsymbol{r}_i$ is simply given by the Coulomb energy,

$$E_{\text{es}} = \frac{1}{4\pi\epsilon_o} \sum_{i,j}^{N} \frac{q_i^* q_j^*}{|\boldsymbol{r}_i - \boldsymbol{r}_j|}, \tag{9}$$

and depends on the effective atomic charges q_i^*, while ϵ_o is the permittivity of free space. If there are no atomic charges, E_{es} disappears and the non-electrostatic contribution E_{bonded} prevails.

2.2.1. *Charge-transfer analysis: Mulliken charges*

In order to analyse how effective point charges can vary with nearest neighbour distance and coordination, density-functional theory (DFT) calculations can provide valuable insights. In principle, the electron density between the nuclei has to be partitioned in a way that each nucleus has a fractional number of electrons associated with it. By adding this number and the nuclear charge one obtains the net atomic charge. A widely used method for performing population analysis has been proposed by Mulliken [38]. All of the electron density in an orbital, represented by the diagonal elements of the density matrix, is allocated to the atom on which the orbital is located. The off-diagonal elements are assigned in equal halves to the respective overlapping orbitals. Although this scheme has some shortcomings, it is in

some respects, a close relative of the algorithm presented here, since charges associated with overlap population are equally divided between pairs of atoms.

We have carried out a set of DFT calculations using the plane-wave code CASTEP [39] and analysed the Mulliken charges for the B1, B2 and zincblende structure at various lattice constants. The results are shown in Figure 1. The data decay exponentially as a function of the interatomic distance and show no saturation for short spacings. Most importantly, there is only a weak variation with the coordination number, which cannot be described with a linear additive model.

In order to rationalise whether the effective charges as predicted by the Mulliken scheme are physically meaningful, a consistency check can be established based on the energy difference of the zincblende and wurtzite structure of GaN, which has been calculated by Stampfl et al. [40].

If we assume that the local charge transfer is determined by the local atomic environment within this first neighbour shell, the effective charges should be almost identical in zincblende and wurtzite structures, since the nearest neighbour distances are basically the same. Consequently, the electrostatic contributions to the interatomic potential could be directly calculated from the Madelung energies of both lattice types, if the effective charges were known. In return, knowing the energy difference, we can determine the effective charges at an equilibrium distance

$$q^* \approx \sqrt{\frac{(E_{\mathrm{coh}}^{\mathrm{W}} - E_{\mathrm{coh}}^{\mathrm{ZB}})r_o}{\alpha^{\mathrm{W}} - \alpha^{\mathrm{ZB}}}}, \tag{10}$$

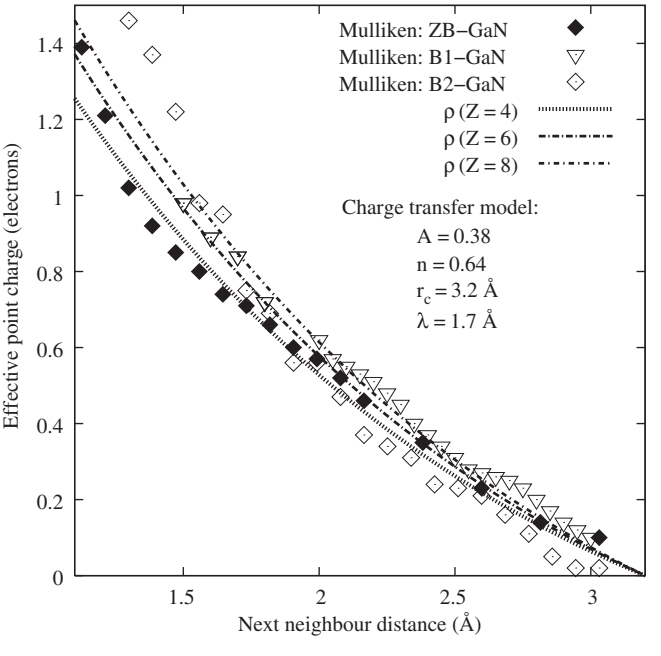

Figure 1. Mulliken charge-transfer analysis for GaN in B1, B2 and zincblende structure. The lines show the fit to the analytical charge-transfer model.

if we assume that the bond lengths are the same for w-GaN and c-GaN. In fact, the different Madelung energies shift the minimum of total potential slightly. This is, however, a very small effect that does not substantially affect the validity of Equation (10). The Madelung constant for wurtzite is $\alpha^{W} = 1.64132$ and for zincblende $\alpha^{ZB} = 1.63806$. The corresponding differences in formation energy are 0.008 eV/f.u. using the LDA approximation [40]. From Equation (10), we obtain a corresponding effective charge of 0.577e for a given bond length of $r_o = 1.9548$ Å. This is in perfect agreement with the result of the Mulliken analysis of our DFT calculations.

2.2.2. *Charge-transfer model*

The charge-transfer model is based on the assumption that charge transfer occurs only among nearest neighbours. Suppose two initially isolated neutral atoms like Ga and N were to approach one another and form a chemical bond. Then a certain amount of charge is transferred between both atoms, which is dependent on the distance and electronegativity of both atoms. The charge transfer is symmetric in the sense that the effective charge gained by one atom (i.e. nitrogen) is counterbalanced by an opposite charge on the other atom (i.e. gallium). If both atoms are the same, there is no charge transfer.

The amount of charge that is transferred between a pair of atoms depends on the distance and is given by a pairwise anti-symmetric charge-transfer function $\rho(r_{ij}) = -\rho(r_{ji})$, which we choose to mimic the effective point charges shown in Figure 1,

$$\rho(r_{ij}) = A \exp\left(-\frac{r_{ij} - r_c}{\lambda} - 1\right)(\delta_{m_i m_j} - 1)^{m_i}, \tag{11}$$

where A, r_c and λ are adjustable parameters, while m_i is the type index of atom i, which is an even integer for cations and an odd integer for anions. The parameter r_c determines the locality of the charge-transfer process, while the Kronecker delta switches the charge-transfer function off for bonds between like atoms.

The effective charge per atom is then a non-linear function of the bond charges, which need to be weighted a quantity of P_{ij} that can be understood as a measure for the electronegativity of the direct environment:

$$P_{ij} = \left(1 + \sum_{k \neq i,j} \rho(r_{ik})/\rho(r_{ij})\right)^{-1/2n}. \tag{12}$$

The effective charge on atom i finally reads

$$q_i^* = \sum_{j \neq i} \frac{P_{ij} + P_{ji}}{2} \rho(r_{ij}). \tag{13}$$

3. Parameter optimisation

The potential parameters are adjusted for the interactions of Ga-Ga, N-N and Ga-N, separately. Since the even bonds are not affected by the charge-transfer scheme, we

adopt the Ga-Ga and N-N parameters as published in [31] in the context of a short-ranged bond-order potential for GaN.

3.1. *Gallium nitride*

The construction of the Ga-N interaction parameters involves the electrostatic and the bonded part. As explained earlier, the parameters for the charge-transfer model (A, r_c, λ and n) are determined by fitting to the Mulliken charges for different interatomic distances and coordinations. After this is done, the fitting of the remaining parameters for the bonded terms can be carried out by using a regular fitting scheme [29,36]. The input data consist of a modified reference data set from DFT-LDA calculations [31], where the electrostatic contributions have been subtracted in the following way: For each structure with coordination number Z ($Z = 1$, 4, 6 and 8) and nearest neighbour separation $r_0(Z)$, the effective charges are calculated from Equations (11)–(13). Using the known Madelung sums for each structure one can then analytically calculate the electrostatic contribution E_{es} to the potential energy, which can be added directly to the bonded contribution E_{bonded} to give the total cohesive energy/formula unit E_{coh}/f.u. After this modification, the fitting of the energies and distances can otherwise be carried out as for an ordinary non-ionic bond-order potential.

The fitted energies and reference data are shown in Figure 2 in comparison to the short-ranged bond-order potential [31]. The charge-transfer model allows us to distinguish the cohesive energies of zincblende and wurtzite, but does not provide an improved description of the B1 and B2 structures as compared to the short-range potential.

The analysis of electrostatic and bonded contributions to the cohesive energy for the various structures under consideration provides interesting insights into the model (Figure 2). We see that, in all structures, the bonded and electrostatic contributions to the cohesive energy are of similar magnitude, with increasing relative contributions of the electrostatic energies at higher coordinations ($Z = 4$–6) (see Figure 3).

Similarly, the equation-of-state for the zincblende phase is shown in Figure 4. Here we analyse the volume dependence of both energy contributions. In contrast to the QEq scheme, there is no softening of the Coulomb terms at shorter distances, but increasing electrostatic energy contributions at smaller volumes due the the exponential distance dependence of the charge-transfer function ρ.

For the four-fold coordinated zincblende structure at the equilibrium distance, we obtain an ionicity ($E_{\mathrm{es}}/E_{\mathrm{coh}}$) of about 42%, in agreement with the usual estimates of an ionicity of about 50% in GaN.

Table 1 shows the fitted energies and bond lengths as well as the results of the fit. Also shown are the effective charges for each equilibrium distance r_0, which are directly comparable to the charges obtained from the Mulliken analysis. The choices of the reference data used are discussed in detail in [31]. Note, especially, that thanks to the inclusion of the electrostatic part, the wurtzite–zincblende energy difference in our model is in practically perfect agreement with the LDA data.

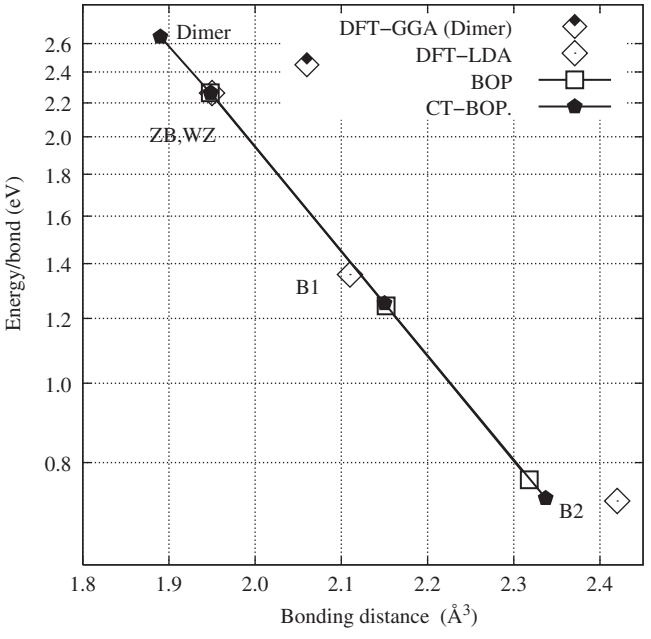

Figure 2. Energy/bond vs. bonding distance for various structure of GaN, including the dimer, wurtzite, zincblende, B1 and B2 phases. Shown are the DFT-LDA reference data set, the short-range bond-order potential [31] and the dynamic charge-transfer bond-order model.

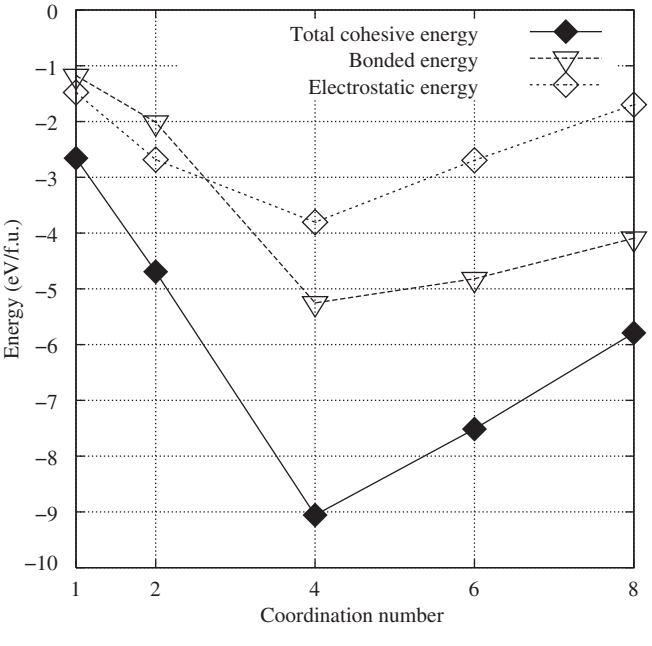

Figure 3. Contributions of the electrostatic and bonded energy terms to the total cohesive energy as a function of the coordination number.

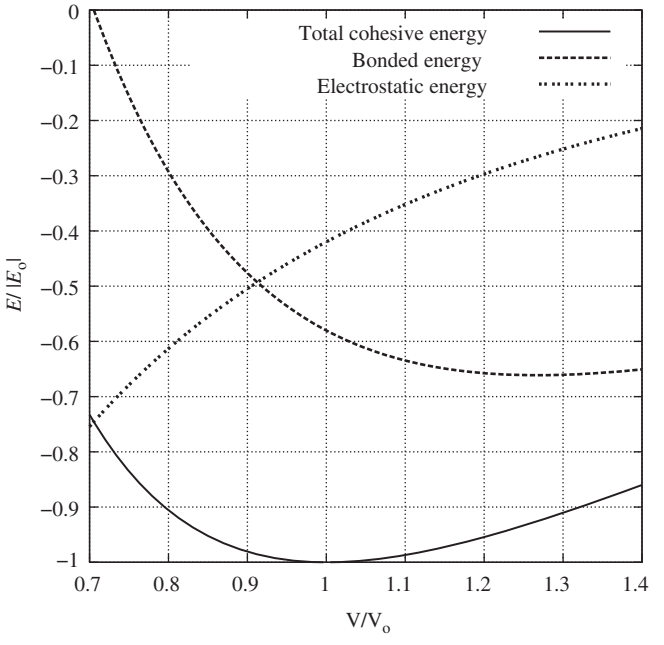

Figure 4. Electrostatic and bonded energy contributions to the energy-volume curve of GaN in zincblende structure.

3.1.1. *Elastic properties*

The fitting of the elastic constants in the charge-transfer scheme needs a conceptually similar modification to the fitting of the energies. The purely ionic contribution of the shear moduli is determined first, and this is, during the fit, added to the covalent contribution to obtain a total modulus which is fitted to the reference data.

The elastic moduli of wurtzite GaN have been studied experimentally [44–46] and theoretically [47–50] by a number of groups. Their results are listed in Table 2 and show significant deviations. This is most likely due to the fact that internal strain leads to atomic relaxations, which is treated differently by the relaxation procedures applied. Therefore, we decided to fit the potential parameters to the elastic properties of zincblende GaN, where only the shear modulus c_{44} is affected by internal strain, and then to validate the results for *w*-GaN.

For fitting the elastic moduli, we have used the static elastic moduli for zincblende GaN as given by Shimada et al. [50]. With the final parameter set, all tensor components were calculated directly by molecular statics allowing for full internal relaxations. The good agreement of the zincblende internal strain parameter ζ with the most recent DFT calculations [50] show that our model also properly describes the internal relaxations. The results compared to the transformation method and literature data are given in Table 2. All elastic moduli are well reproduced within the uncertainty limits of the reference data. The relative differences of directly calculated values and those obtained by the transformation procedure are most significant for c_{44}.

Table 1. Energy and structural parameters of different GaN phases. Given are experimental values and theoretical results from DFT calculations in comparison to the corresponding numbers as described with the analytical model. The q values give the charge per atom (positive for Ga, negative for N) at the equilibrium separation r_o of the corresponding structure. The wurtzite structure has $u = 3/8$.

GaN dimer	LCAO [41]	Exp. (from [42])	BOP [31]	DCT-BOP
r_o (Å)	2.06		1.921	1.891
D_o (eV)	2.45		2.45	2.657
$q(r_o)$				0.441
Zincblende GaN	LDA [42]			
a_o (Å^3)	4.497	4.50	4.498	4.500
E_{coh}/f.u. (eV)	9.048		9.056	9.050
B (GPa)	196		205	202
B'	4.2		4.14	4.5
$q(r_o)$				0.559
Wurtzite GaN				
a_o (Å^3)	3.180	3.190	3.180	3.179
c/a	1.632	1.627	1.633	1.636
r_o (Å^3)	1.948	1.956	1.948	1.948
u	0.376	0.377	0.375	0.375
E_{coh}/f.u. (eV)	9.058	9.058	9.056	9.057
B (GPa)	196	188–245	205	202
B'	4.3	3.2–4.3		
$q(r_o)$				0.560
B1	LDA [43]			
a_o (Å^3)	4.225		4.304	4.302
E_{coh}/f.u. (eV)	8.150		7.460	7.514
B (GPa)	240		233	232
B'	4.5		4.7	4.6
$q(r_o)$				0.480
B2				
a_o (Å^3)	2.802		2.676	2.699
E_{coh}/f.u. (eV)	5.75		6.09	5.791
B (GPa)	240		218	218
B'	4.5		5.2	5.2
$q(r_o)$				0.395

3.1.2. *Point defects*

Although there has been much progress in growing GaN during the last decade, there are many open questions related to native point defects and impurities. The sources of n type conductivity and yellow luminescence, for example, are still under discussion, and knowledge of the electronic properties of defects in GaN in general is still far from being complete, although the subject has been the topic of several recent theoretical studies [52–57].

An inherent problem of analytic interatomic potentials is that they do not describe the electronic subsystem and therefore cannot account for the presence of electronic band defects and the fact that defects occur in various charge states

Table 2. Elastic constants for zincblende and wurtzite GaN.

ZB	Calc.[1]	Calc.[2]	Calc.[3]	Exp.[4]	Exp.[5]	Exp.[6]	BP[7]	BOP[8]	DCT-BOP[9]
c_{11}	285	282	293				300	287	281
c_{12}	161	159	159				191	169	164
c_{44}	149	142	155				160	128	128
c'_{44}	202		200					244	204
ζ	0.67	0.5	0.61					0.699	
WZ									
c_{11}	350		367	390	365	377	386	343	337
c_{12}	140		135	145	135	160	160	159	154
c_{13}	104		103	106	114	114	141	123	118
c_{33}	376	405	405	398	381	209	391	379	374
c_{44}	101		95	105	109	81.4	115	72	71
c_{66}	115		116	123	115	109	113	92	92

[1]LDA pseudopotential calculation [50]
[2]FP-LMTO LDA calc. [48]
[3]LDA pseudopotential calculation [49]
[4]Brillouin scattering [44]
[5]Brillouin scattering [45]
[6]Resonance ultrasound [46]
[7]Coulomb–Buckingham potential [51]
[8]Analytic bond-order potential [31]
[9]This work

depending on the Fermi energy level. Therefore, such potentials are of very limited use for a thermodynamic understanding of the defect chemistry of solids. However, it is a worthwhile task to characterise the potential properties also with respect to point defects, since they can occur in molecular dynamics simulations under non-equilibrium conditions. As compared to fixed charge models, the charge-transfer scheme presented here has the advantage that charge neutrality is maintained even for non-stoichiometric compositions, and therefore we restrict ourselves to the case of neutral defects.

The basic goal was to reproduce the hierarchy in formation energies of the different neutral point defects, which are, to a large extent, determined by the significant difference in the atomic covalent radii of nitrogen and gallium atoms. Defects were investigated for a system that was thermally equilibrated at 600 K and then slowly cooled down to 0 K at zero pressure. The defect formation energy E_F then was determined from the potential energy E_D of the cell containing the defect following the formalism of Qian et al. [58]. The calculated defect formation energies are given in Table 3 for the nitrogen rich limit.

The potential describes the nitrogen vacancy well, which is the most important point defect in GaN. Also, the other vacancies and interstitials are reproduced with reasonably accuracy considering the uncertainties of the reference data. Only the formation energy of the N antisite is suspiciously high.

Although, currently, all of the defects have local charge neutrality as explained above, we note that it would be possible to extend the model to deal with charged defects by explicitly adding a charge state on atoms or on a vacant site.

Table 3. Defect formation energies E_F for the main point defects in GaN. The values are for N-rich conditions. Energies are given in eV, formation volumes in Å^3. The column non-ionic gives the results for our earlier non-ionic model. [31]

Defect	E_F current work	E_F non-ionic	E_F [1]	E_F [2]	E_F [3]
V_{Ga}	4.4	4.4	6.8		6.3
V_N	2.1	1.4	1.2		4.6
Ga_N	3.8	3.0	6.8		10.5
N_{Ga}	10.6	5.2	5.2	5.7	5.8
I_N	7.3	5.7	3.2		
I_{Ga}	8.1	5.5	4.1		

[1]LDA-DFT pseudopot. calc. [52]
[2]LDA-DFT pseudopot. calc., calculated in ZB [54,55]
[3]DFT-LMTO calc. [56]

3.1.3. *Melting point*

The melting point of GaN is somewhat uncertain due to experimental difficulties related to the very high temperature and N_2 pressure necessary for melting. Experiments in a high pressure anvil cell showed that GaN does not melt at temperatures as high as 2573 K at 68 kbar [59]. A CALPHAD (CALculation of PhAse Diagrams) method thermodynamic analysis of available experimental data predicts a melting temperature of 2792 K at equilibrium pressure of N_2 [60]. We determined the melting point of the simulated model, firstly to find out that it is not unrealistically low compared to the experimental assessments, secondly, since a melting simulation carried out with the liquid–solid equilibrium method [61] serves as a good test, that the potential does not have artificial minima [62].

Using the liquid–solid equilibrium method we found that the melting point of GaN in the current model is 3500 ± 500 K. The high uncertainty is due to the high computational cost of simulating the ionic model for the long time-scales required to find thermodynamic equilibrium. This is in reasonable agreement with the analytical estimate of the melting point of 2791 K at 45 kbar [63] and 2792 K from the CALPHAD method [60].

3.2. *Practical implementation*

The practical implementation of the current model requires three components (which, in practice, are subroutines in a computer program). The covalent bonding part can be treated with a subroutine for calculating the potential energy for Tersoff-like potentials. Such routines are widely available. The charge transfer requires another, entirely new routine which outputs the charge of each atom. Once the charges are calculated, the long-range Coulombic interaction can be calculated with any of the several methods available for this purpose, for instance Ewald mesh methods [64,65] or fast multipole methods [66–68]. Also, truncated Coulomb potentials can be used, although then care should be taken that this does not lead to

any of the known problems with potential truncation [69]. In the end, the covalent bond and ionic energies are simply summed together.

For calculation of the potential energy only, the above approach is straightforward. To also calculate the interatomic forces (necessary for MD simulations), a complication arises in that the atomic charges depend on the interatomic distances, and hence give rise to force components not present in a fixed-charge model [70]. The Appendix presents a detailed derivation of these force components. With use of the additional neighbour list described in the Appendix, these forces can be added to the long-range force calculation scheme without major modification of the code. The charge-transfer/force calculation subroutine is available from one of the authors (KN).

In our code, we used a covalent force subroutine based on one originally developed by Morris et al. [71] and heavily modified to be able to deal with compounds and our modifications to the Tersoff functional form [72]. The long-range forces were handled with the DPMTA method [67] which is a linear-scaling fast multipole method. In a few cases, when high accuracy was desired, we noticed that numerical 'noise' in this method prevented getting very accurate results. In such cases, the final energy was evaluated with a brute-force direct summation of the Coulomb interaction over symmetrically placed increasingly distant image cells. The brute force approach was also used in the nanocluster simulations, since no periodic image cells are needed and the direct summation is therefore exact when all pairs are summed over.

The charge-transfer subroutine is comparable in efficiency with the covalent bond (Tersoff) one, but any Coulomb potential calculation scheme is much slower than either of these. Hence, our charge-transfer scheme does not cause any significant slowdown of the code when compared to other methods with explicit ionic charges.

4. Applications: irradiation effects

The irradiation of materials with high energy (keV or MeV) ions can lead to dramatic modification of the material. It is well known that a single keV ion irradiation event can melt the material locally for a few ps, produce hundreds of defects, and for most ceramic materials, cause a crystalline-to-amorphous phase transition (see e.g. [73] and references therein). It is also known that damage in highly ionic materials often differs dramatically from that in covalent and metallic ones. For instance, the amorphisation dose of GaN is one to three orders of magnitude higher than that in GaAs [74,75]. Hence, it is a natural question to ask whether the ionic bonding itself can be the reason to this difference. Since in an ionic material defects can be charged, it is plausible that defects far from each other are subject to the long-range ionic interactions, which could affect defect recombination strongly. Our previous non-ionic model for GaN [31] and the present one are fitted to the same database and are of comparable quality with respect to the reproduction of crystalline phases, elasticity and defect properties. Hence, simulating irradiation effects with both of them provides an ideal way to test whether including explicit ionic interactions affects the primary state of damage during ion irradiation.

We carried out the testing in two different stages. We first simulated the damage produced by single high-energy recoils in GaN. Such recoils can be experimentally produced inside a material with MeV electron, neutron or light ion irradiation.

The defects produced in 400 eV and 1 keV cascades for both models are shown in Table 4. It is evident that the the non-ionic and ionic models predict very similar damage production in the recoil events. Because of the large statistical uncertainties, we cannot rule out that there might be some difference in the number of antisites, but it is clear that the difference is not an order-of-magnitude one.

Computer capacity limitations prevented us from simulating large numbers of higher-energy cascades, which are known to produce liquid-like zones and amorphisation in semi-conductors [76]. But to mimic heat spikes in a better-defined system than the chaotic and extended cascades, we simulated a test system manufactured as follows: A simulation cell consisting of 8192 atoms at perfect lattice sites was set up. The atoms closer than 10 Å to the centre of the cell were given an initial velocity in random directions. The velocity was selected so that the cell heated up to about 2000 K after reaching thermal equilibrium. This way the centre of the cell heated up quickly and produced a molten zone, which then partially recrystallised. The number of disordered atoms against time is given in Figure 5 for the long- and short-range models. Again, the behaviour is very similar. A molten region of about 800 atoms is produced in the centre of the cell. The disordered region quickly recrystallises, and after 2 ps, there are about 100 disordered atoms remaining.

These results show, somewhat surprisingly, that the inclusion of explicit ionic interactions does not affect damage production in GaN. This negative finding is significant in that (if it proves to be valid in other materials as well) it shows that the long-range effects of ionicity on the bonding can be well compensated by a computationally much more efficient short-range model for modelling of the primary state of radiation damage. It also indicates that the difference between the primary state of irradiation damage in ionic and non-ionic materials is at least not explicitly caused by the ionic interactions.

Table 4. Damage produced by 400 eV and 1 keV recoils with short- and long-range models. The number of defects is a sum of the defects in both Ga and N sublattices.

Energy	Vacancies	Interstitials	Antisites
		Short-range	
400 eV	2.8 ± 0.4	2.8 ± 0.4	0.66 ± 0.2
1 keV	6.3 ± 0.7	6.3 ± 0.7	2.1 ± 0.4
		Long-range	
400 eV	3.0 ± 1.2	3.0 ± 1.2	0*
1 keV	6.3 ± 1.1	6.3 ± 1.1	3.3 ± 0.3

*Antisites were not observed in the five 400 eV simulations.

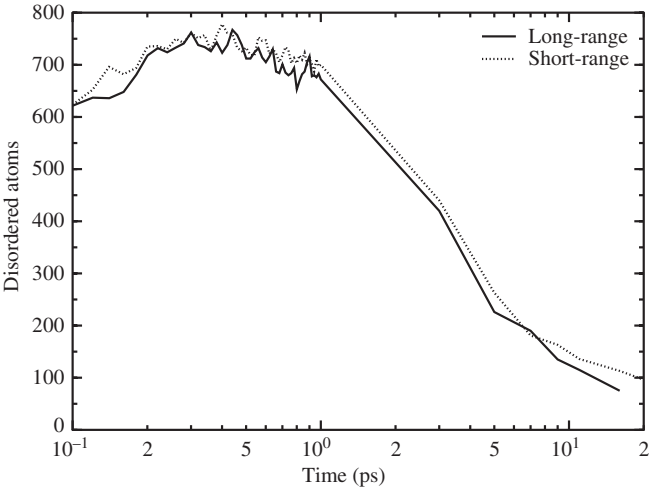

Figure 5. Number of disordered atoms vs. time after high energy density melt in crystalline GaN modelled with the ionic long-range and non-ionic short-range potential models.

5. Summary

We have presented an analytical dynamic charge-transfer scheme that reproduces the distance and coordination dependence of Mulliken charges in gallium nitride as obtained from an analysis of total energy DFT calculations. The basic concepts derive from the idea of bond charges. We assume pairwise symmetric charge transfer between odd atom types forming a bond. Charge contributions of all bonds are individually weighted by the electronegative strength and summed up, which yields the effective charge per atom, while maintaining overall charge neutrality. The method is used to complement a short-ranged bond-order potential for the ionic-covalent gallium nitride. The potential is fully analytic and computationally efficient as compared to alternative schemes based on the QEq method, without suffering from problems with energy conservation or shielding effects. By comparing defect production rates for 400 eV and 1 keV recoils as obtained from MD simulations using the ionic and a short-ranged bond-order potential no appreciable differences are found.

Acknowledgements

Dr. Roy Benedek, Argonne National Laboratory, is thanked for fruitful discussions in the early stages of this work. The German Academic Exchange Service (DAAD) and the Finnish Academy are thanked for providing a travel grant to the authors of this paper.

References

[1] A. Carlsson, *Solid State Physics*, *Advances in Research and Applications*, Vol. 43, Academic Press, New York, 1990.
[2] G. Lewis and C. Catlow, J. Phys. C 18 (1985) p.1149.
[3] S. Rick and S. Stuart, Rev. Comp. Chem. 18 (2002) p.89.

[4] R. Sanderson, Science 114 (1951) p.670.
[5] J. Perdew, R. Parr, M. Levy and J.L. Baldus Jr., Phys. Rev. Lett. 49 (1982) p.1961.
[6] W. Mortier, S. Gosh and S. Shankar, J. Am. Chem. Soc. 108 (1986) p.4315.
[7] A.K. Rappé and W. Goddard III, J. Phys. Chem. 95 (1991) p.3358.
[8] S. Rick, S. Stuart and B. Berne, J. Chem. Phys. 101 (1994) p.6141.
[9] S. Valone and S. Atlas, J. Chem. Phys. 120 (2004) p.7262.
[10] F. Streitz and J. Mintmire, Thin Solid Films 253 (1994) p.179.
[11] F. Streitz and J. Mintmire, Phys. Rev. B 50 (1994) p.11996.
[12] F. Streitz and J. Mintmire, LANGMUIR 12 (1996) p.4605.
[13] S. Ogata, H. Iyetomi, K. Tsuruta, F. Shimojo, R. Kalia, A. Nakano and P. Vashishta, J. Appl. Phys. 86 (1999) p.3036.
[14] X. Zhou, H. Wadley, J. Filhol and M. Neurock, Phy. Rev. B 69 (2004) p.035402.
[15] A. Duinvan, A. Strachan, S.S.Q. Zhangan, X. Xu and W.A. Goddard III, J. Phys. Chem. A 107 (2003) p.3803.
[16] W.A. Goddard III, Q. Zhang, M. Ulodogan, A. Strachan and T. Cagin, *The ReaxFF polarizable reactive force field for molecular dynamics simulation of ferroelectrics*, in *Fundamental Physics of Ferroelectrics*, R.E. Cohen, ed., AIP, Melville, New York, 2002, p.45.
[17] B. Thomas, N. Marks and B. Begg, Phys. Rev. B 69 (2004) p.144122.
[18] B.S. Thomas and N.A. Marks, Phys. Rev. B 76 (2007) p.167401.
[19] A. Yasukawa, JSME Int. J. Series A Mech. Mater. Eng. 39 (1996) p.313.
[20] J. Yu, S.B. Sinnott and S.R. Phillpot, Phys. Rev. B 75 (2007) p.085311.
[21] T. Iwasaki and H. Miura, J. Mater. Res. 16 (2001) p.1789.
[22] R. Tetot, A. Hallil, J. Creuze and I. Braems, Eur. Phys. Lett. 83 (2008) p.40001.
[23] J. Goniakowski and C. Noguera, Surf. Sci. 319 (1994) p.81.
[24] X.W. Zhou and F.P. Doty, Phys. Rev. B 78 (2008) p.224307.
[25] A. Alavi, L.J. Alvarez, S.R. Elliott and I.R. McDonald, Phil. Mag. B 65 (1992) p.489.
[26] Z. Jiang and R.A. Brown, Phys. Rev. Lett. 74 (1995) p.2048.
[27] F. Stillinger and T. Weber, Phys. Rev. B 31 (1985) p.5262.
[28] K. Muralidharan, C. Cao, Y.X. Wan, K. Runge and H.P. Cheng, Chem. Phys. Lett. 437 (2007) p.92.
[29] P. Erhart and K. Albe, Phys. Rev. B 71 (2005) p.035211.
[30] K. Albe, K. Nordlund, J. Nord and A. Kuronen, Phys. Rev. B 66 (2002) p.035205.
[31] J. Nord, K. Albe, P. Erhart and K. Nordlund, J. Phys. Condens. Matter. 15 (2003) p.5649.
[32] K. Albe, K. Nordlund and R. Averback, Phys. Rev. B 65 (2002) p.195124.
[33] M. Mueller, P. Erhart and K. Albe, J. Phys. Condens. Mat. 19 (2007) p.326220.
[34] N. Juslin, P. Erhart, P. Traskelin, J. Nord, K. Henriksson, K. Nordlund, E. Salonen and K. Albe, J. Appl. Phys. 98 (2005) p.123520.
[35] D. Brenner, Phys. Rev. Lett. 63 (1989) p.1022.
[36] K. Albe, K. Nordlund and R. Averback, Phys. Rev. B 65 (2002) p.195214.
[37] K. Albe, K. Nordlund, J. Nord and A. Kuronen, Phys. Rev. B 66 (2002) p.035205.
[38] R. Mulliken, J. Chem. Phys. 36 (1962) p.3428.
[39] *Cerius2 Users Guide*, Accelrys, San Diego, 2002.
[40] C. Stampfl and C. de Wallevan, Phys. Rev. B 59 (1999) p.5521.
[41] A. Kandalam, R. Pandey, M. Blanco, A. Costales, J. Recio and J. Newsam, J. Phys. Chem. B 104 (2000) p.4361.
[42] J. Serrano, A. Rubio, E. Hernández, A. Muñoz and A. Mujica, Phys. Rev. B 62 (2000) p.16612.
[43] A. Muñoz and K. Kune, Phys. Rev. B 44 (1991) p.10372.
[44] A. Polian, M. Grimsditch and I. Grzegory, J. Appl. Phys. 79 (1996) p.3343.
[45] M. Yamaguchi, T. Yagi, T. Azuhata, T. Sota, K. Suzuki, S. Chichibu and S. Nakamura, J. Phys. Condens. Matter 9 (1997) p.241.

[46] R. Schwarz, K. Khachaturyan and E. Weber, Appl. Phys. Lett. 70 (1997) p.1122.
[47] K. Kim, W. Lambrecht and B. Segall, Phys. Rev. B 53 (1996) p.16310.
[48] K. Kim, W. Lambrecht and B. Segall, Phys. Rev. B 56 (1997) p.7018.
[49] A.F. Wright, J. Appl. Phys. 82 (1997) p.2833.
[50] K. Shimada, T. Sota and K. Suzuki, J. Appl. Phys. 84 (1998) p.4951.
[51] P. Zapol, R. Pandey and J. Gale, J. Phys. Condens. Matter 9 (1997) p.9517.
[52] J. Neugebauer and C.G.V.D. Walle, Phys. Rev. B 50 (1994) p.8067.
[53] P. Boguslawski, E.L. Briggs and J. Bernholc, Phys. Rev. B 51 (1995) p.17255.
[54] T. Mattila, A. Seitsonen and R.M. Nieminen, Phys. Rev. B 54 (1996) p.1474.
[55] T. Mattila and R.M. Nieminen, Phys. Rev. B 55 (1997) p.9571.
[56] I. Gorczyca, A. Svane and N.E. Christensen, Phys. Rev. B 60 (1999) p.8147.
[57] I. Gorczyca, A. Svane and N. Christensen, Solid State Comm. 101 (1997) p.747.
[58] G.X. Qian, R. Martin and D. Chadi, Phys. Rev. B 38 (1988) p.7649.
[59] J. Edgar, *Properties of Group III-Nitrides*, INSPEC, London, 1994.
[60] A.V. Davydov and T.J. Anderson, *Thermodynamic analysis of the Ga-N system*, in *III-V Nitride Materials and Processes III*, T.D. Moustakas, S.E. Mohney and S.J. Pearton, eds., ECS, Boston, MA, 1998, pp.38–49.
[61] J.R. Morris, C.Z. Wang, K.M. Ho and C.T. Chan, Phys. Rev. B 49 (1994) p.3109.
[62] K. Nordlund and A. Kuronen, Nucl. Instr. Meth. Phys. Res. B 159 (1999) p.183.
[63] J.A.V. Vechten, Phys. Rev. B 7 (1973) p.1479.
[64] P.A. Batcho, D.A. Case and T. Schlick, J. Chem. Phys. 115 (2001) p.4003.
[65] T. Darden, L. Pedersen, A. Toukmaji, M. Crowley and T. Cheathan, *Proceedings of the Eighth SIAM Conference on Parrallel Processing for Scientific Computing*, PPSC (1997) p.1.
[66] R.K. Kalia, A. Nakano, A. Omeltchenko, K. Tsuruta and P. Vashishta, *Chemistry and physics of nanostructures and related non-equilibrium materials*, in *Million Atom Molecular Dynamics Simulation of Nanophase Silicon Nitride*, E. Ma, B. Fultz, R. Shull, J. Morral and P. Nash, eds., TMS, Warrendale, PA, 1997, pp.89–96.
[67] W.T. Rankin and J.J.A. Board, *A portable distributed implementation of the parallel multipole tree algorithm*, in *Proceedings of the 1995 IEEE Symposium on High Performance Distributed Computing*, IEEE Computer Society Press, Los Alamitos, California, 1995, pp.17–22.
[68] L. Greengard and V. Rokhlin, J. Comput. Phys. 73 (1987) p.325.
[69] M. Patra, M. Karttunen, M. Hyvonen, E. Falck, P. Lindqvist and I. Vattulainen, Eur. Biophys. J. 32 (2003) p.216.
[70] A. Alavi, L.J. Alvarez, R. Elliott and I.R. MacDonald, Phil. Mag. B 65 (1992) p.489.
[71] J.R. Morris, AL_CMD, code available at http://cmp.ameslab.gov/cmp/CMP_Theory/cmd/cmd.html.
[72] K. Albe, K. Nordlund and R.S. Averback, Phys. Rev. B 65 (2002) p.195124.
[73] R.S. Averback and T. Diaz de la Rubia, *Displacement damage in irradiated metals and semiconductors*, in *Solid State Physics*, H. Ehrenfest and F. Spaepen, eds., Academic Press, New York, 1998, pp.281–402.
[74] E. Wendler, A. Kamarou, E. Alves, K. Gärtner and W. Wesch, Nucl. Instr. Meth. Phys. Res. B 206 (2003) p.1028.
[75] S.O. Kucheyev, J.S. Williams, C. Jagadish, J. Zou, G. Li and A.I. Titov, Phys. Rev. B 64 (2001) p.035202.
[76] M.W. Bench, I.M. Robertson and M.A. Kirk, Nucl. Instr. Meth. Phys. Res. B 59/60 (1991) p.372.
[77] J.A. Board, C.W. Humphres, C.G. Lambert, W.T. Rankin and A.Y. Toukmaji, *Proceedings of the Eighth SIAM Conference on Parrallel Processing for Scientific Computing*, PPSC (1997) p.1.

Appendix: Calculating forces from the charge-transfer potential

The total potential energy of an N atom system due to the charge-transfer potential is calculated from (in units with $1/(4\pi\epsilon_0) = 1$)

$$V_{\mathrm{ct}} = \frac{1}{2} \sum_s \sum_{t \neq s} \frac{q_s q_t}{r_{st}}, \tag{A1}$$

where

$$q_s = \sum_{u \neq s} \frac{P_{su} + P_{us}}{2} \rho(r_{su}) \tag{A2}$$

$$P_{su} = \left(1 + \sum_{v \neq s,u} \frac{\rho(r_{sv})}{\rho(r_{su})} \right)^{-1/2n} \tag{A3}$$

$$\rho(r_{su}) = A \left(e^{-\frac{r_{su} - r_c}{\lambda}} - 1 \right) (-1)^{\delta_{s,\,\mathrm{Nitrogen}}}. \tag{A4}$$

The meaning of the terms is discussed in the main text of the paper. All sums described in this appendix loop over all atoms $1, \ldots, N$ in the system, except when otherwise specified below the sum sign.

To calculate the force $\boldsymbol{F}_i$ acting on atom i, we have to calculate

$$_i = -\nabla_{\boldsymbol{r}_i} \frac{1}{2} V_{\mathrm{ct}} = -\nabla_{\boldsymbol{r}_i} \frac{1}{2} \sum_s \sum_{t \neq s} \frac{q_s q_t}{r_{st}}. \tag{A5}$$

Contrary to the case of an ordinary Coulomb potential, where q_s and q_t are constant, in the charge-transfer case they depend on the coordinates of the nearby atoms. Hence, the derivative $\nabla_{\boldsymbol{r}_i}$ has to be applied on all terms q_s, which depend on the coordinates of atom i. In other words, we have to find all terms in the sum where either q_s, q_t or r_{st} depend on $\boldsymbol{r}_i$. Using the rule for a derivative of a product, we get

$$_i = -\frac{1}{2} \sum_s \sum_{t \neq s} \left(q_s q_t \, \nabla_{\boldsymbol{r}_i} \frac{1}{r_{st}} + \frac{(\nabla_{\boldsymbol{r}_i} q_s) q_t}{r_{st}} + \frac{q_s (\nabla_{\boldsymbol{r}_i} q_t)}{r_{st}} \right). \tag{A6}$$

The derivative of r_{st} gives the usual forces acting between constant charged bodies. For q_s, we have to note that if either s, u, or v in Equations (A2)–(A4) is equal to i, there will be a force contribution from the term $\nabla_{\boldsymbol{r}_i} q_s$, and similarly for q_t.

Because the sum loops over all (s, t) pairs twice, the latter two terms in Equation (A6) are equivalent on the exchange of s and t, and we can write

$$\boldsymbol{F}_i = -\frac{1}{2} \sum_s \sum_{t \neq s} \left(\underbrace{-\frac{q_s q_t}{r_{st}^2} \hat{\boldsymbol{r}}_{st}}_{s=i \text{ or } t=i} + 2 \frac{(\nabla_{\boldsymbol{r}_i} q_s) q_t}{r_{st}} \right) \tag{A7}$$

$$= -\frac{1}{2} \sum_s \sum_{t \neq s} \left(\underbrace{-2 \frac{q_s q_t}{r_{st}^2} \hat{\boldsymbol{r}}_{st}}_{s=i} + 2 \frac{(\nabla_{\boldsymbol{r}_i} q_s) q_t}{r_{st}} \right) \tag{A8}$$

$$= -\sum_s \sum_{t\neq s} \left(\underbrace{-\frac{q_s q_t}{r_{st}^2}\hat{\boldsymbol{r}}_{st}}_{s=i} + \underbrace{\frac{(\nabla_{r_i} q_s) q_t}{r_{st}}}_{\text{Any } s \text{ for which } (\nabla_{r_i} q_s)\neq 0} \right). \tag{A9}$$

The first part is just the derivative of the Coulomb potential in a system with no charge transfer.

Evaluating the latter part requires care. As stated above, q_s is a three-body function, and hence $\nabla_{r_i} q_s$ may be non-zero even when $s \neq i$. Thus, the sum can contain terms of the type

$$\frac{(\nabla_{\boldsymbol{r}_i} q_s) q_t}{r_{st}}, \quad i \neq s \neq t, \tag{A10}$$

which complicates practical evaluation: one needs to keep track of $\nabla_{\boldsymbol{r}_i} q_s$ pairwise for (i, s) to know which r_{st} one should use. And even atoms which are not neighbours of s, but only neighbours w of a neighbour u of s, can contribute to the force on atom i.

To find out for which terms $\nabla_{\boldsymbol{r}_i} q_s \neq 0$, we first need to fully evaluate

$$\nabla_{\boldsymbol{r}_i} q_s = \nabla_{\boldsymbol{r}_i} \left(\sum_{u\neq s} \frac{P_{su} + P_{us}}{2} \rho(r_{su}) \right) \tag{A11}$$

$$= \nabla_{\boldsymbol{r}_i} \left(\sum_{u\neq s} \frac{\left(1 + \sum_{v\neq s,u} \frac{\rho(r_{sv})}{\rho(r_{su})}\right)^{-1/2n} + \left(1 + \sum_{w\neq u,s} \frac{\rho(r_{uw})}{\rho(r_{us})}\right)^{-1/2n}}{2} \rho(r_{su}) \right). \tag{A12}$$

Now we find that there are, in total, four atoms in the sum which may be the atom i and hence contribute to the force on atom i: s, u, v or w.

Derivative of q_s

Continuing from Equation (A13),

$$\nabla_{\boldsymbol{r}_i} q_s = \frac{1}{2} \nabla_{\boldsymbol{r}_i} \sum_{u\neq s} \left[\left(1 + \sum_{v\neq s,u} \frac{\rho(r_{sv})}{\rho(r_{su})}\right)^{-1/2n} + \left(1 + \sum_{w\neq u,s} \frac{\rho(r_{uw})}{\rho(r_{us})}\right)^{-1/2n} \right] \rho(r_{su}) \tag{A13}$$

$$\begin{aligned} = \frac{1}{2} \sum_{u\neq s} & \left[\nabla_{\boldsymbol{r}_i} \left(1 + \sum_{v\neq s,u} \frac{\rho(r_{sv})}{\rho(r_{su})}\right)^{-1/2n} + \nabla_{\boldsymbol{r}_i} \left(1 + \sum_{w\neq u,s} \frac{\rho(r_{uw})}{\rho(r_{us})}\right)^{-1/2n} \right] \rho(r_{su}) \\ & + \left[\left(1 + \sum_{v\neq s,u} \frac{\rho(r_{sv})}{\rho(r_{su})}\right)^{-1/2n} + \left(1 + \sum_{w\neq u,s} \frac{\rho(r_{uw})}{\rho(r_{us})}\right)^{-1/2n} \right] \nabla_{\boldsymbol{r}_i} \rho(r_{su}) \end{aligned} \tag{A14}$$

$$\begin{aligned} = \frac{1}{2} \sum_{u\neq s} & \left[\overbrace{\frac{-1}{2n} \left(1 + \sum_{v\neq s,u} \frac{\rho(r_{sv})}{\rho(r_{su})}\right)^{-1/2n-1}}^{\equiv P_{su}^d} \left(\nabla_{\boldsymbol{r}_i} \sum_{v\neq s,u} \frac{\rho(r_{sv})}{\rho(r_{su})} \right) + \right. \\ & \left. \overbrace{\frac{-1}{2n} \left(1 + \sum_{w\neq u,s} \frac{\rho(r_{uw})}{\rho(r_{us})}\right)^{-1/2n-1}}^{\equiv P_{us}^d} \left(\nabla_{\boldsymbol{r}_i} \sum_{w\neq u,s} \frac{\rho(r_{uw})}{\rho(r_{us})} \right) \right] \rho(r_{su}) \end{aligned} \tag{A15}$$

$$
\begin{aligned}
&+[P_{su}+P_{us}]\nabla_{\mathbf{r}_i}\rho(r_{su})\\
&=\frac{1}{2}\sum_{u\neq s}\Bigg[P^d_{su}\left(\sum_{v\neq s,u}\frac{\rho(r_{su})(\nabla_{\mathbf{r}_i}\rho(r_{sv}))-\rho(r_{sv})(\nabla_{\mathbf{r}_i}\rho(r_{su}))}{\rho(r_{su})^2}\right)\\
&\quad+P^d_{us}\left(\sum_{w\neq u,s}\frac{\rho(r_{us})(\nabla_{\mathbf{r}_i}\rho(r_{uw}))-\rho(r_{uw})(\nabla_{\mathbf{r}_i}\rho(r_{us}))}{\rho(r_{us})^2}\right)\Bigg]\rho(r_{su}) \qquad \text{(A16)}\\
&\quad+[P_{su}+P_{us}]\nabla_{\mathbf{r}_i}\rho(r_{su}). \qquad \text{(A17)}
\end{aligned}
$$

Here the atom configuration can be illustrated as follows:

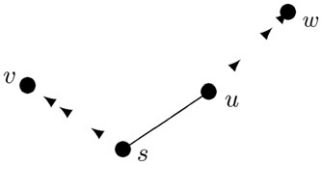

i.e. w is a neighbour of v but not necessarily s.

Now this can be handled depending on which index s, u, v or w equals i. In the following, we handle the four cases separately:

(A) $\boldsymbol{s=i}$

$$
\begin{aligned}
\nabla_{\mathbf{r}_i}q_i&=\frac{1}{2}\sum_{u\neq i}\Bigg[P^d_{iu}\left(\sum_{v\neq i,u}\frac{\rho(r_{iu})(\nabla_{\mathbf{r}_i}\rho(r_{iv}))-\rho(r_{iv})(\nabla_{\mathbf{r}_i}\rho(r_{iu}))}{\rho(r_{iu})^2}\right)\\
&\quad+P^d_{ui}\left(\sum_{w\neq u,i}\frac{\rho(r_{ui})(\nabla_{\mathbf{r}_i}\rho(r_{uw}))-\rho(r_{uw})(\nabla_{\mathbf{r}_i}\rho(r_{ui}))}{\rho(r_{ui})^2}\right)\Bigg]\rho(r_{iu})\\
&\quad+[P_{iu}+P_{ui}]\nabla_{\mathbf{r}_i}\rho(r_{iu})\\
&=\frac{1}{2}\sum_{u\neq i}P^d_{iu}\left(\sum_{v\neq i,u}\frac{\rho(r_{iu})(\nabla_{\mathbf{r}_i}\rho(r_{iv}))-\rho(r_{iv})(\nabla_{\mathbf{r}_i}\rho(r_{iu}))}{\rho(r_{iu})^2}\right)\rho(r_{iu})\\
&\quad+P^d_{ui}\left(\sum_{w\neq u,i}\frac{-\rho(r_{uw})(\nabla_{\mathbf{r}_i}\rho(r_{ui}))}{\rho(r_{ui})^2}\right)\rho(r_{iu})\\
&\quad+\left[P_{iu}\nabla_{\mathbf{r}_i}\rho(r_{iu})+P_{ui}\nabla_{\mathbf{r}_i}\rho(r_{iu})\right].
\end{aligned}
\qquad \text{(A18)}
$$

(B) $\boldsymbol{u=i}$

$$
\begin{aligned}
\nabla_{\mathbf{r}_i}q_s&=\frac{1}{2}\sum_{i\neq s}\Bigg[P^d_{si}\left(\sum_{v\neq s,i}\frac{\rho(r_{si})(\nabla_{\mathbf{r}_i}\rho(r_{sv}))-\rho(r_{sv})(\nabla_{\mathbf{r}_i}\rho(r_{si}))}{\rho(r_{si})^2}\right)\\
&\quad+P^d_{is}\left(\sum_{w\neq i,s}\frac{\rho(r_{is})(\nabla_{\mathbf{r}_i}\rho(r_{iw}))-\rho(r_{iw})(\nabla_{\mathbf{r}_i}\rho(r_{is}))}{\rho(r_{is})^2}\right)\Bigg]\rho(r_{si})\\
&\quad+[P_{si}+P_{is}]\nabla_{\mathbf{r}_i}\rho(r_{si})\\
&=\frac{1}{2}\sum_{i\neq s}P^d_{si}\left(\sum_{v\neq s,i}\frac{-\rho(r_{sv})(\nabla_{\mathbf{r}_i}\rho(r_{si}))}{\rho(r_{si})^2}\right)\rho(r_{si})\\
&\quad+P^d_{is}\left(\sum_{w\neq i,s}\frac{\rho(r_{is})(\nabla_{\mathbf{r}_i}\rho(r_{iw}))-\rho(r_{iw})(\nabla_{\mathbf{r}_i}\rho(r_{is}))}{\rho(r_{is})^2}\right)\rho(r_{si})\\
&\quad+\left[P_{si}\nabla_{\mathbf{r}_i}\rho(r_{si})+P_{is}\nabla_{\mathbf{r}_i}\rho(r_{si})\right].
\end{aligned}
\qquad \text{(A19)}
$$

(C) $\boldsymbol{v}=\boldsymbol{i}$

$$\begin{aligned}\nabla_{\boldsymbol{r}_i} q_s = &\frac{1}{2}\sum_{u\neq s}\Bigg[P^d_{su}\left(\sum_{i\neq s,u}\frac{\rho(r_{su})(\nabla_{\boldsymbol{r}_i}\rho(r_{si}))-\rho(r_{si})(\nabla_{\boldsymbol{r}_i}\rho(r_{su}))}{\rho(r_{su})^2}\right)\\ &+P^d_{us}\left(\sum_{w\neq u,s}\frac{\rho(r_{us})(\nabla_{\boldsymbol{r}_i}\rho(r_{uw}))-\rho(r_{uw})(\nabla_{\boldsymbol{r}_i}\rho(r_{us}))}{\rho(r_{us})^2}\right)\Bigg]\rho(r_{si})\\ &+[P_{su}+P_{us}]\nabla_{\boldsymbol{r}_i}\rho(r_{su})\\ =&\frac{1}{2}\sum_{u\neq s}P^d_{su}\left(\sum_{i\neq s,u}\frac{\rho(r_{su})(\nabla_{\boldsymbol{r}_i}\rho(r_{si}))}{\rho(r_{su})^2}\right)\rho(r_{su}).\end{aligned}\tag{A20}$$

(D) $\boldsymbol{w}=\boldsymbol{i}$

$$\begin{aligned}\nabla_{\boldsymbol{r}_i} q_s = &\frac{1}{2}\sum_{u\neq s}\Bigg[P^d_{su}\left(\sum_{v\neq s,u}\frac{\rho(r_{su})(\nabla_{\boldsymbol{r}_i}\rho(r_{sv}))-\rho(r_{sv})(\nabla_{\boldsymbol{r}_i}\rho(r_{su}))}{\rho(r_{su})^2}\right)\\ &+P^d_{us}\left(\sum_{i\neq u,s}\frac{\rho(r_{us})(\nabla_{\boldsymbol{r}_i}\rho(r_{ui}))-\rho(r_{ui})(\nabla_{\boldsymbol{r}_i}\rho(r_{us}))}{\rho(r_{us})^2}\right)\Bigg]\rho(r_{su})\\ &+[P_{su}+P_{us}]\nabla_{\boldsymbol{r}_i}\rho(r_{su})\\ =&\frac{1}{2}\sum_{u\neq s}P^d_{us}\left(\sum_{i\neq u,s}\frac{\rho(r_{us})(\nabla_{\boldsymbol{r}_i}\rho(r_{ui}))}{\rho(r_{us})^2}\right)\rho(r_{su}).\end{aligned}\tag{A21}$$

For practical implementation in a computer program, one can reduce the number of sums to a single (*ijk*) three-body loop by using the following transformations. We handle the P_{su}, $\sum_v$ loop as *ijk* and P_{us}, $\sum_w$ also as *ijk*. We use the transformations

$$\text{for } P_{su},\ \sum_v : \begin{matrix} s & u & v \\ \downarrow & \downarrow & \downarrow \\ i & j & k \end{matrix} \quad \text{and for} \quad P_{us},\ \sum_w : \begin{matrix} u & s & w \\ \downarrow & \downarrow & \downarrow \\ i & j & k \end{matrix}.\tag{A22}$$

This also determines which atom the force acts on: for instance, for the case $u=i$, the force will act on either atom j (P_{su}) or atom i (P_{us}). After these transformations, several of the derivative terms given above become identical and can be combined.

Finally, we note that the neighbour lists should be constructed such that they also contain the far neighbours w as seen from atom s.

We tested that our derivative works correctly by comparing with numerical derivation in parabolic approximation (three points). Using purely numerical means, we found that one can get $\sim$eight-digit accuracy in the numerical derivative, providing for stringent testing of the analytical derivative. We progressed in the testing from simple to more complicated systems, starting from a dimer (tests two-body parts only), and continuing with two dimers separated by more than r_c (tests two-body parts plus long-range part), a linear trimer (tests three-body part in simplest possible manner), and finally in random nanocluster and bulk atom configurations. In the final version of the subroutine, perfect agreement between the analytical and numerical derivative was achieved within the $\sim$ eight-digit numerical accuracy for all these cases.

When the charge-transfer scheme is implemented in a Ewald mesh [64] or field multipole method [77] the charge-transfer force terms need to be added to the force evaluation of the summation scheme.